1052–1058 *Nucleic Acids Research, 2018, Vol. 46, No. 3* *Published online 20 December 2017*
doi: 10.1093/nar/gkx1267

Triggering nucleic acid nanostructure assembly by conditional kissing interactions

Laurent Azéma[1,*], Servane Bonnet-Salomon[1], Masayuki Endo[2,3], Yosuke Takeuchi[2], Guillaume Durand[1], Tomoko Emura[2], Kumi Hidaka[2], Eric Dausse[1], Hiroshi Sugiyama[2,3] and Jean-Jacques Toulmé[1,*]

[1]University of Bordeaux, CNRS UMR 5320, INSERM U1212, Bordeaux 33076, France, [2]Department of Chemistry, Graduate School of Science, Kyoto University, Kyoto 606-8502, Japan and [3]Institute for Integrated Cell-Material Science, Kyoto University, Kyoto 606-8501, Japan

Received July 12, 2017; Revised November 17, 2017; Editorial Decision December 06, 2017; Accepted December 07, 2017

ABSTRACT

Nucleic acids are biomolecules of amazing versatility. Beyond their function for information storage they can be used for building nano-objects. We took advantage of loop–loop or kissing interactions between hairpin building blocks displaying complementary loops for driving the assembly of nucleic acid nano-architectures. It is of interest to make the interaction between elementary units dependent on an external trigger, thus allowing the control of the scaffold formation. To this end we exploited the binding properties of structure-switching aptamers (aptaswitch). Aptaswitches are stem–loop structured oligonucleotides that engage a kissing complex with an RNA hairpin in response to ligand-induced aptaswitch folding. We demonstrated the potential of this approach by conditionally assembling oligonucleotide nanorods in response to the addition of adenosine.

INTRODUCTION

Molecular interaction pattern and shape driven by their primary sequence make nucleic acids of particular interest for the design of spatially controlled nano-architectures (1,2). Since the pioneering work of Seeman (3), who used Holliday junctions as structural elements (4) and constructed cube (5), many nucleic acid nanostructures have been depicted: triangle (6), grid (7), square (8), ring (9), tetrahedron (10) or bricks (11). In 2006, the M13 bacteriophage folding method proposed by Rothemund paved the way to origami design of nanostructures (12). These 3D structures (13,14) were engineered for monitoring molecular interactions (15–17), drug delivery (18,19), or as protein assembly template (20,21).

Watson–Crick base-pairing between complementary oligonucleotides drives the assembly of the constitutive modules of such nanoscaffolds. This is generally achieved through the formation of 15–25 nucleotide long duplexes. A particular case results from the use of hairpin building blocks displaying complementary loops, giving rise to loop–loop interaction, so-called kissing complexes. Taking advantage of such interactions a polyhedron was previously designed from tRNA-derived modules (22,23). Besides naturally occurring kissing complexes (24,25), hairpin RNA pairs were identified through aptamer selection (26,27) against RNA motifs (28–30). Both the loop sequence and the nature of loop closing residues ensure a high affinity (nanomolar range) and a high specificity of recognition (31–33). RNA/DNA (34,35) and DNA/DNA (36) kissing hairpin pairs were also described.

For many diverse applications (sensing, delivery, nanomachines) it is of interest to drive the assembly/disassembly of nucleic acid-based nanostructures by an external trigger. Nanodevices can act as actuators, upon addition of an input molecule (37–39) or pH change (40,41), or can present a target-dependent folding (42–44). Recently, Willner *et al.* reported the disassembly of origami tiles upon ligand-induced aptamer conformational change (45). Binding of aptamers to their targets is known to generally occur through induced-fit (46). Structural changes associated to aptamer-target complex formation were exploited for engineering molecular beacons and for the design of new selection procedures (47–49).

An aptaswitch is an aptamer in equilibrium between at least two different conformations. We explored the potential of kissing aptaswitches, i.e. of aptamers folded as imperfect hairpins whose apical loop is prone to generate a kissing complex with a second hairpin named aptakiss (50–

*To whom correspondence should be addressed. Tel: +33 557571016; Fax: +33 557571014; Email: laurent.azema@u-bordeaux.fr
Correspondence may also be addressed to Jean-Jacques Toulmé. Email: jean-jacques.toulme@inserm.fr
Present address: Guillaume Durand, Bordeaux Science Agro, Gradignan 33170, France.

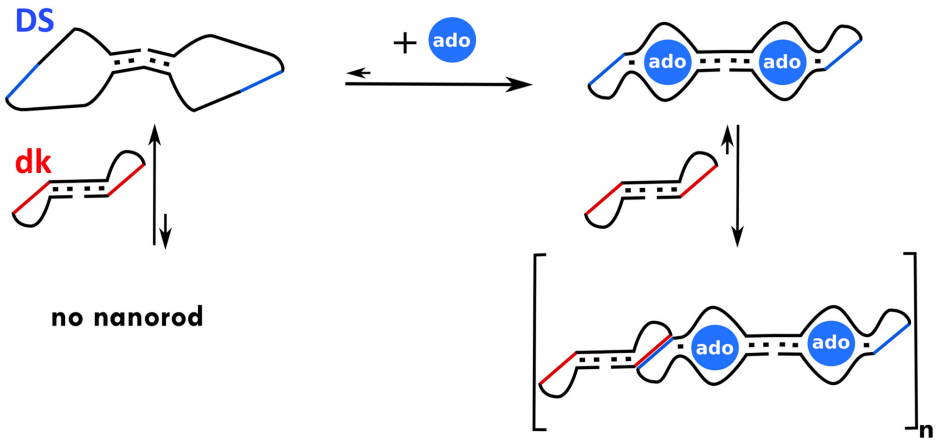

Figure 1. Principle of conditional nanorod formation. The double-aptaswitch (DS) is in equilibrium between two structures (top line) upon the addition of adenosine (ado). The apical loops (blue) of the ado–bound structure engages kissing interaction with the loops (red) of the double-aptakiss (dk) leading to the formation of the nanorod. In the absence of adenosine no kissing takes place.

53). Upon addition of its cognate target molecule, the aptamer switches from an unfolded to a folded structure corresponding to free and target-bound forms, respectively. The kissing complex is strongly favored with the folded compared to the unfolded aptaswitch (50). Consequently the addition of the target molecule triggers the aptakiss–aptaswitch association. We aimed at exploiting this property for driving the building of nanostructures through the addition of a trigger molecule (Figure 1). We report here the adenosine-dependent specific association of kissing aptaswitch/aptakiss building blocks.

MATERIALS AND METHODS

Oligonucleotides toolbox

Oligonucleotides were synthesized and purified according to standard procedures (see supporting information for detailed protocols). A set of oligonucleotides, consisting in monomers and dimers of aptakiss and aptaswitch and their controls was prepared (Supplementary Table S1). Secondary structure were predicted using mfold software (54). Analysis without constraint, at 20°C, 100 mM NaCl and 10 mM Mg^{2+} gave the most stable secondary structure. Then constraints were applied, in order to free the apical kissing loop. The resulting structures are schematized in Figure 2 (55).

Electrophoretic mobility shift assay

Sample preparation. Oligonucleotides at 10× final concentration and adenosine (varying concentration) were heated at 80°C for 2 min and subsequently chilled 5 min on ice. 5X SE buffer (100 mM AcONa, 0.7 M AcOK, 50 mM $Mg(OAc)_2$, 0.5 M HEPES, pH 7.5) was added to the oligonucleotide and solutions were incubated for 15 min. Oligonucleotides were adjusted to the desired final concentration in 1X SE buffer, in a total volume of 10 μL.

Electrophoresis. Oligonucleotide complexes were run on polyacrylamide gels (acrylamide/bis-acrylamide 19/1 (v/v) 40% stock solution) at a final percentage of 8%. Adenosine was added to the solution (final concentration 0–8 mM) in TAC buffer 1X (10 mM $Mg(OAc)_2$, 50 mM Tris pH 7.5). Polymerisation was initiated by addition of 1 vol.% ammonium persulfate and 0.1 vol.% TEMED. Samples were loaded after dilution in 10 μl of Native Loading Buffer (NLB: 15% glycerol (m/v), 0.5 mg/ml bromophenol blue in TAC 1X buffer). Migration was performed at 4°C, 150 V, on a refrigerated Owl P10DS (Thermo®) electrophoretic system connected to a cooled bath.

Silver nitrate staining. Protocol was adapted from the literature (56). After electrophoresis, oligonucleotides were fixed by dipping the gel into 300 ml of 7.5% acetic acid, for 15 min. Acetic acid solution was discarded and the gel was dipped into 300 ml of 15% formaldehyde in water for 15 min. Solution was then discarded and gel was dipped into 300 ml of silver nitrate (1 $g.L^{-1}$ in water), for 30 min at room temperature, shielded from light. Silver nitrate solution was removed; the gel was rinsed with water and allowed to stand at 4°C in 300 ml of aqueous developing solution (8% (w/v) Na_2CO_3, 0.05% $Na_2S_2O_3$ (v of 25 mM stock solution/v), until satisfying band revelation. Staining was stopped and fixed by dipping the gel into a final 7.5% acetic acid solution, for 10 min.

Fluorescence anisotropy

Anisotropy measurements were carried out on a Tecan® Infinite M1000 plate reader, monitored through Tecan Infinite® software. The fluorescence anisotropy (r) was calculated as:

$$r = \frac{I_{\parallel} - I_{\perp}}{I_{\parallel} + 2I_{\perp}}$$

where $I_{//}$ and $I_{\perp}$ are respectively the parallel and perpendicular polarized components of the emission after excitation by perpendicular polarized light. The fluorescence anisotropy change (Δr) was calculated as: $\Delta r = r - r_0$, where r_0 is the fluorescence anisotropy of the 3′ Texas Red®-labeled aptakiss k_{TR} ($\lambda_{Exc} = 590$ nm; $\lambda_{Em} = 635$ nm) alone

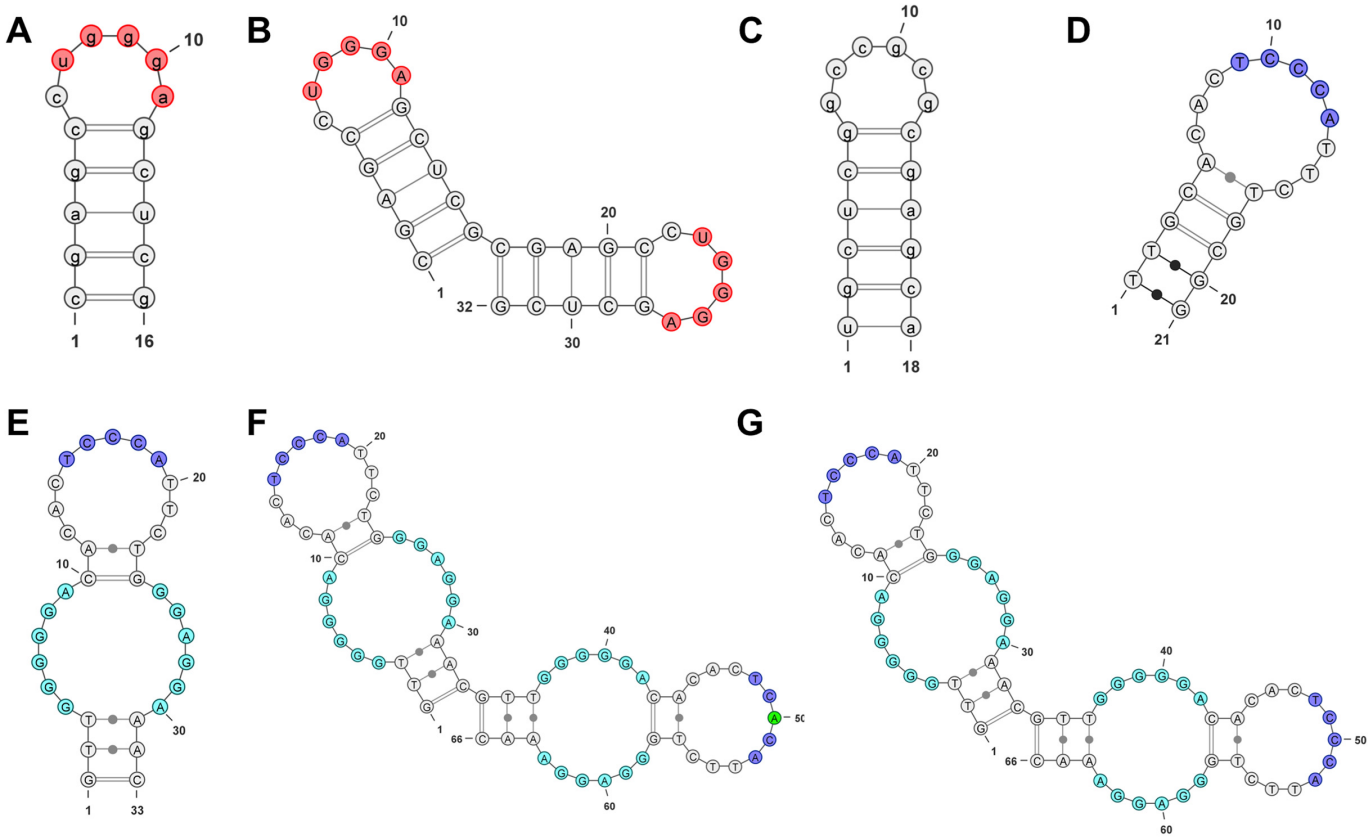

Figure 2. Oligonucleotide toolbox. (**A**) aptakiss k; (**B**) double aptakiss dk; (**C**) control aptakiss k_m, which doesn't bind to L; (**D**) hairpin L with a complementary loop to k; (**E**) adenoswitch S' (**F**) mutated double adenoswitch DS_{mut}; (**G**) double adenoswitch DS. Color code. Cyan blue**:** adenosine recognition internal loop; blue**:** kissing motif in S, L or DS loop; red**:** kissing motif in k or dk loop; green**:** point mutation, preventing kissing complex formation.

and *r* is the fluorescence anisotropy of k_{TR} at a given analyte concentration. Samples were dispensed in 96 well plates (Lo bind flatblack Greiner®). The total sample volume of 100 μl was obtained by mixing solutions 1 and 2 (50 μl of each). Solution 1: k_{TR} (20 nM final) in 1X SE buffer. Solution 2: aptaswitch (2X final concentration) and adenosine (2X concentration according to the assay). Solutions 1 and 2 (oligonucleotides + water) were heated for 2 min at 80°C and then chilled 5 min on ice. SE buffer (1X final concentration) and adenosine (2X final concentration) were added and the resulting solution was incubated 15 min at room temperature. Solutions 1 and 2 were dispensed in a 96-well plate (total volume of the assay = 100 μl/well). The plate was sealed and stored at 4°C for 4 h before readout.

AFM analysis

AFM images were obtained on a high-speed AFM (Nano-Live Vision, RIBM, Tsukuba, Japan) using a silicon nitride cantilever (Olympus BL-AC10EGS). Samples were prepared by following the previously described method (57). The sample (2 μl) was absorbed on a mica plate pretreated with 0.1% aminopropyl-triethoxysilan for 5 min at room temperature, and then washed with the same buffer solution for the experiment. Scanning was performed in the same buffer solution using a tapping mode.

RESULTS AND DISCUSSION

Aptakiss/aptaswitch dimers

We first engineered a DNA adenoswitch (Figure 2E and Supplementary Table S1) by substituting a previously characterized DNA kissing motif (34) to the apical loop of a previously identified adenosine aptamer (58) as in our study, we used adenosine as the trigger molecule. The secondary structure of the adenosine DNA aptamer was demonstrated to be structured as an imperfect stem–loop with a central loop (59) that interacts with two adenosine molecules. The apical loop is not involved in the recognition of adenosine and can thus be modified. The DNA sequence 5′-CACTCCCATTC that was previously shown to give rise to stable kissing interaction with an RNA hairpin was chosen (34) and flanked by the α and β closing base pairs A-T and C-G that were shown to be important for correct loop folding (60) (Supplementary Figure S2). This adenoswitch specifically responds to the simultaneous addition of adenosine and of an RNA aptakiss k (Figure 2A) displaying a 5′CUGGGA loop (61). Two structures at least of the aptaswitch, folded and unfolded, respectively, are in equilibrium, where only the folded one is able to engage a kissing complex with its aptakiss partner (Supplementary Figure S1). In the absence of the target, the equilibrium is shifted toward the unfolded structure unable to interact with the aptakiss. The addition of adenosine, drives the equilibrium

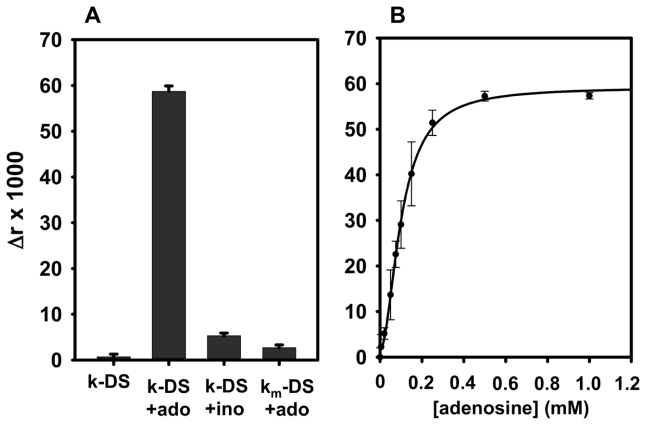

Figure 3. Evaluation of the adenosine-dependent binding properties of the double aptaswitch DS to the aptakiss k_{TR} by fluorescence anisotropy. (**A**) k_{TR}: Texas Red-conjugated aptakiss (10 nM); ado: adenosine (1 mM); ino: inosine (1 mM); k_{mTR}: Texas Red®-conjugated aptakiss variant (10 nM); DS: double adenoswitch (100 nM). (**B**) Binding curve of DS to k, as a function of adenosine concentration. Concentrations of k and DS as in A. See supporting information for methods and sequences (Supplementary Table S1).

in favour of the folded structure able to form a kissing complex. In order to propagate the adenoswitch-aptakiss complex the elementary modules should contain two interacting sites (Figure 1). Head to tail (3′ to 5′) dimers of both the RNA aptakiss (dk) and of the DNA adenoswitch (DS) were thus designed (Figure 2B and G) that can potentially form a 5 base-pair loop–loop interaction on either side (Supplementary Figure S3). Using fluorescence anisotropy, we firstly monitored the binding properties of DS to k_{TR}, a Texas red®-labelled monomer aptakiss k (Figure 3).

An increased fluorescence anisotropy of k_{TR} was observed upon addition of DS in the presence of 1 mM adenosine whereas no variation was detected in the absence of the ligand (Figure 3A). The observed Δr (+64 mp) was specific: indeed, when inosine that is not recognized by the parent aptamer was substituted to adenosine, the anisotropy variation was very low ($\Delta r = +5$ mp). Moreover, the use of k_m (53), an RNA hairpin (Figure 2C), which does not bind to the DS apical loop (Supplementary Figure S6A) does not induce any anisotropy variation ($\Delta r = +2$ mp). Taken together these results demonstrate the adenosine-dependent formation of a DS–k kissing complex. Figure 3B presents the binding curve of DS to k, as a function of the adenosine concentration. Non-linear fit gave an apparent K_D value of 101.5 ± 3.7 μM, which is related to the affinity of the adenoswitch for adenosine, in the k–DS–Ado ternary complex. Indeed, the equilibrium dissociation constant of the complex formed by k and L, a DNA hairpin containing the apical loop of DS (Supplementary Figure S6B), is in the low nanomolar range ($K_D < 0.5$ nM), as well as the one for the DS-k interaction at saturating concentration of adenosine ($K_D = 9$ nM) (Supplementary Figure S6C). All experiments above were performed at 10 mM magnesium, which is a saturating concentration, as we determined a K_D of 470 μM for the DS–k interaction as a function of Mg^{2+} concentration under saturating adenosine conditions (Supplementary Figure S6D).

Nanorod: electrophoretic mobility shift assay

We next monitored the adenosine-dependent association of the double adenoswitch DS with the double aptakiss dk by non-denaturing polyacrylamide gel electrophoresis. In the absence of adenosine, dk migrated as a single band (Figure 4A, lane 1).

In contrast several discrete bands were observed for DS that likely correspond to different conformations (Figure 4A, lane 2); the one that shows the highest mobility is the most intense. The electrophoretic pattern of the DS+dk mixture is the superimposition of the individual patterns of the two constituents (Figure 4A, lane 3). We then run the same three samples on a gel in which adenosine was added to the acrylamide/bis-acrylamide solution prior to polymerization (Figure 4C). In this case, the pattern for the DS + dk mixture shows a low mobility band (lane 3) that appeared to the expense of the ones characteristic of DS and k, except for the DS low mobility band that remains unaffected; this is indicative of a species in slow equilibrium with the structure engaged in the kissing complex under these experimental conditions. The upper band in Figure 4C, lane 3 can be ascribed to a DS–dk complex, that we call nanorod. The weak staining of this band in lane 3 compared to the intensity of the 2 DS and dk bands in lanes 1 and 2 can be ascribed to the formation of supramolecular assemblies of different sizes. Indeed it looks scattered as expected for a mixture of species with slightly different mobilities. In addition, depending on the stability of the association, complexes might dissociate during the migration; the smear observed below the upper band suggests that it is likely the case. This nanorod complex is dependent on and specific of adenosine: the migration of the DS–dk mixture on an inosine-containing gel did not give rise to any retarded band (Figure 4B, lane 3) whereas the high mobility bands of individual DS and dk species remain visible.

Additional band shift assays were carried out in order to check whether the complex formation was controlled by the adenosine concentration as expected from our model. A smear was observed above the intense DS band at an adenosine concentration as low as 0.1 mM (Supplementary Figure S4, lane B3) indicating the formation of a species that dissociates during the migration. The smear extended toward the upper part of the gel as the adenosine concentration increased over the 0.5 - 8 mM range to the expense of the DS and dk bands. Concomitantly material accumulated at the top of the gel in a scattered band, the mobility of which decreased when the adenosine concentration increased. This is consistent with an increased amount of DS–dk supramolecular complex and an increased size of putative nanorods as adenosine concentration increases. In order to check that the low mobility band observed for the DS–dk mixture in the presence of adenosine actually contains adenoswitch–aptakiss polymers we synthesized modules displaying only one interacting loop in order to generate different complexes of defined size. The combination of DS with k or dk and that of DS_{mut} (adenoswitch mutated in one loop thus preventing kissing interaction on that side) with k or dk led to a single band of the relative expected mobility (Supplementary Figure S5), indicating the formation of defined molecular species. All these complexes that

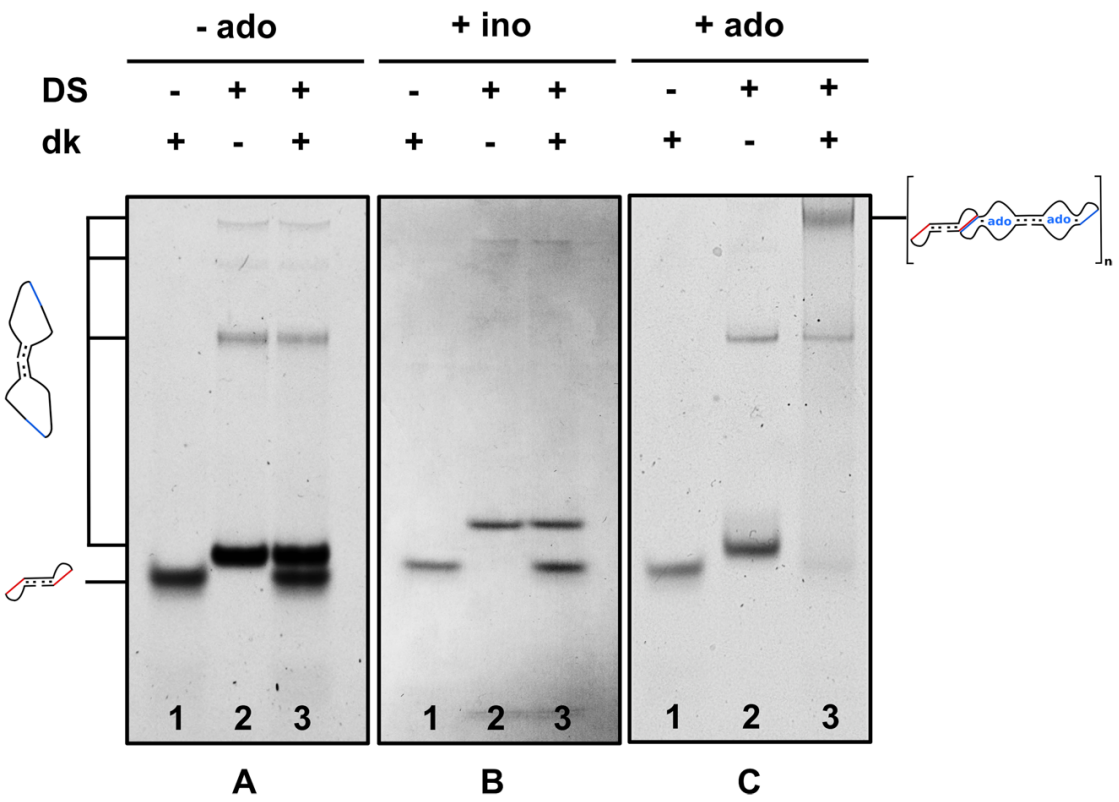

Figure 4. Non-denaturing PAGE shift assay of adenosine-dependent kissing complexes *(silver nitrate staining)*. DS and dk (2 μM each) were run alone in lanes 1 and 2, respectively, and together (lanes 3) (**A**). In the absence of adenosine (ado), or (**B**). in the presence of inosine (ino, 8 mM) in the gel, or (**C**). in the presence of adenosine (8 mM) in the gel.

involved at most 3 building units (DS_{mut}–dk–DS_{mut} or k–DS–k; Supplementary Figure S5, lanes 6, 8 and 9) displayed a much higher mobility than the one observed with the DS–dk mixture (Supplementary Figure S5, lanes 10). Consequently, this demonstrates that the $(dk–DS)_n$ complex involves more than two modules.

Nanorod: atom force microscopy

We then attempted to visualize adenosine-dependent nanorod complexes by atomic force microscopy (AFM). Typical images obtained with a DS + dk mixture folded in absence or in presence of inosine (as a control) or adenosine are shown on Figure 5.

Short bent structures were seen exclusively in the presence of adenosine (right panel). Kissing complexes can display a kinked structure (33); the relative position of the two stems at the exit of the loop–loop helix is highly dependent on the length of this helix and on the number of unpaired residues at the junction between the stem and the loop–loop helix. Indeed we observed highly variable mobility for different RNA–RNA kissing complexes of the same size, indicating different conformations likely reflecting different shapes from co-linear to sharply broken complexes (unpublished results) This might account for the bent shape seen for the DS–dk nanorods (Figure 5, right panel). A DS–dk binary complex could be roughly assimilated to a 50 bp double-stranded nucleic acid (12 bp for the dk stems + 12 bp for the 2 loop–loop helices + 26 bp for DS (59). A linear duplex of that size is about 17 nm long. From the AFM picture one can roughly evaluate that the nano-objects resulting from the adenosine-induced DS–dk association are about 40–50 nm long, meaning that they comprise no more than three DS–dk modules. Even though it is not possible to evaluate the size of the adenoswitch-aptakiss complexes in the low mobility band seen on polyacrylamide gels (Figure 4C, lane 3; Supplementary Figure S5, lane 10) they likely contain more than 3 modules. It is also amazing that the addition of adenosine led to a remarkable monodisperse distribution of the nanorod size seen by AFM. One cannot exclude that the preparation and or the observation of the samples that involve mechanical stress were detrimental to the persistence of longer polymers.

In conclusion, we demonstrated the interest of aptaswitch/aptakiss complexes for the conditional formation of nucleic acid nanoarchitecture. In order to build object of a larger size, aptaswitch/aptakiss couples could be grafted to large origami structure, these hetero dimers being conditional communication modules. This will benefit from an extended DNA-DNA kissing complexes repertoire, that could be inserted into nanostructures (62) (Dausse *et al.*, unpublished results) allowing to take advantage of Holliday junctions. The combination of two different aptaswitches, in order to get access to logic gates (63–65) can also be considered.

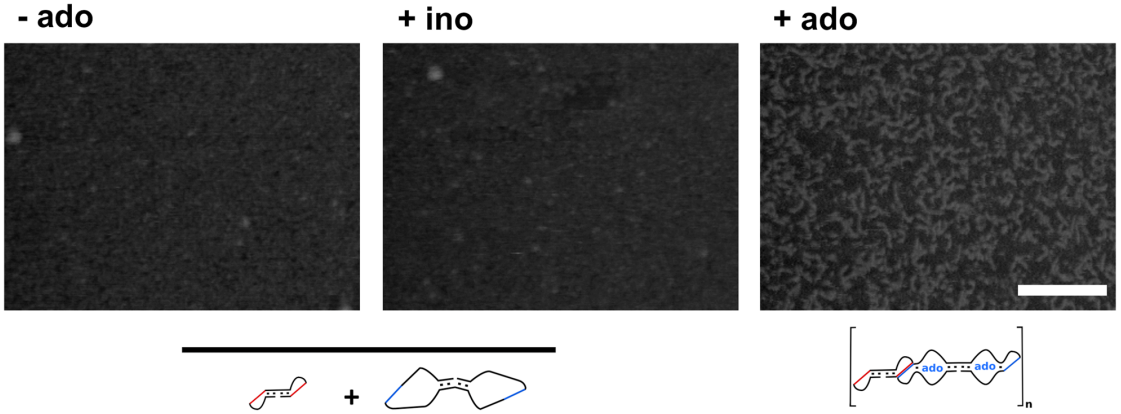

Figure 5. Adenosine-dependent formation of DS–dk nanorods monitored by AFM. Complexes of DS and dk (1.25 μM each) were analyzed in the absence (left) or in the presence of 4 mM of inosine (centre, as a control) or 4 mM adenosine (right). Scale bar: 100 nm.

SUPPLEMENTARY DATA

Supplementary Data are available at NAR online.

ACKNOWLEDGEMENTS

The authors thank the Conseil Régional d'Aquitaine for financial support.

FUNDING

Funding for open access charge: University of Bordeaux and INSERM.
Conflict of interest statement. None declared.

REFERENCES

1. Chandrasekaran,A.R. (2016) Programmable DNA scaffolds for spatially-ordered protein assembly. *Nanoscale*, **8**, 4436–4446.
2. Li,H., Lee,T., Dziubla,T., Pi,F., Guo,S., Xu,J., Li,C., Haque,F., Liang,X.-J. and Guo,P. (2015) RNA as a stable polymer to build controllable and defined nanostructures for material and biomedical applications. *Nano Today*, **10**, 631–655.
3. Seeman,N.C. (2003) DNA in a material world. *Nature*, **421**, 427–431.
4. Seeman,N.C. (1982) Nucleic acid junctions and lattices. *J. Theor. Biol.*, **99**, 237–247.
5. Chen,J. and Seeman,N.C. (1991) Synthesis from DNA of a molecule with the connectivity of a cube. *Nature*, **350**, 631–633.
6. Ohno,H., Kobayashi,T., Kabata,R., Endo,K., Iwasa,T., Yoshimura,S.H., Takeyasu,K., Inoue,T. and Saito,H. (2011) Synthetic RNA–protein complex shaped like an equilateral triangle. *Nat. Nanotechnol.*, **6**, 116–120.
7. Han,D., Pal,S., Yang,Y., Jiang,S., Nangreave,J., Liu,Y. and Yan,H. (2013) DNA gridiron nanostructures based on four-arm junctions. *Science*, **339**, 1412–1415.
8. Jasinski,D.L., Khisamutdinov,E.F., Lyubchenko,Y.L. and Guo,P. (2014) Physicochemically tunable polyfunctionalized RNA square architecture with fluorogenic and ribozymatic properties. *ACS Nano*, **8**, 7620–7629.
9. Ohayon,Y.P., Sha,R., Flint,O., Liu,W., Chakraborty,B., Subramanian,H.K.K., Zheng,J., Chandrasekaran,A.R., Abdallah,H.O., Wang,X. *et al.* (2015) Covalent linkage of one-dimensional DNA arrays bonded by paranemic cohesion. *ACS Nano*, **9**, 10304–10312.
10. Goodman,R.P., Berry,R.M. and Turberfield,A.J. (2004) The single-step synthesis of a DNA tetrahedron. *Chem. Commun.*, **20**, 1372.
11. Ke,Y., Ong,L.L., Shih,W.M. and Yin,P. (2012) Three-dimensional structures self-assembled from DNA bricks. *Science*, **338**, 1177–1183.
12. Rothemund,P.W.K. (2006) Folding DNA to create nanoscale shapes and patterns. *Nature*, **440**, 297–302.
13. Douglas,S.M., Dietz,H., Liedl,T., Högberg,B., Graf,F. and Shih,W.M. (2009) Self-assembly of DNA into nanoscale three-dimensional shapes. *Nature*, **459**, 414–418.
14. Douglas,S.M., Marblestone,A.H., Teerapittayanon,S., Vazquez,A., Church,G.M. and Shih,W.M. (2009) Rapid prototyping of 3D DNA-origami shapes with caDNAno. *Nucleic Acids Res.*, **37**, 5001–5006.
15. Yamagata,Y., Emura,T., Hidaka,K., Sugiyama,H. and Endo,M. (2016) Triple helix formation in a topologically controlled DNA nanosystem. *Chem. - A Eur. J.*, **22**, 5494–5498.
16. Nickels,P.C., Høiberg,H.C., Simmel,S.S., Holzmeister,P., Tinnefeld,P. and Liedl,T. (2016) DNA origami seesaws as comparative binding assay. *ChemBioChem*, **17**, 1093–1096.
17. Godonoga,M., Lin,T.-Y., Oshima,A., Sumitomo,K., Tang,M.S.L., Cheung,Y.-W., Kinghorn,A.B., Dirkzwager,R.M., Zhou,C., Kuzuya,A. *et al.* (2016) A DNA aptamer recognising a malaria protein biomarker can function as part of a DNA origami assembly. *Sci. Rep.*, **6**, 21266.
18. Schaffert,D.H., Okholm,A.H., Sørensen,R.S., Nielsen,J.S., Tørring,T., Rosen,C.B., Kodal,A.L.B., Mortensen,M.R., Gothelf,K. V. and Kjems,J. (2016) Intracellular delivery of a planar DNA origami structure by the transferrin-receptor internalization pathway. *Small*, **12**, 2634–2640.
19. Kohman,R.E., Cha,S.S., Man,H.-Y. and Han,X. (2016) Light-triggered release of bioactive molecules from DNA nanostructures. *Nano Lett.*, **16**, 2781–2785.
20. Chandrasekaran,A.R., Anderson,N., Kizer,M., Halvorsen,K. and Wang,X. (2016) Beyond the fold: emerging biological applications of DNA origami. *ChemBioChem*, **17**, 1081–1089.
21. Yang,Y.R., Liu,Y. and Yan,H. (2015) DNA nanostructures as programmable biomolecular scaffolds. *Bioconjug. Chem.*, **26**, 1381–1395.
22. Severcan,I., Geary,C., Chworos,A., Voss,N., Jacovetty,E. and Jaeger,L. (2010) A polyhedron made of tRNAs. *Nat. Chem.*, **2**, 772–779.
23. Dabkowska,A.P., Michanek,A., Jaeger,L., Rabe,M., Chworos,A., Höök,F., Nylander,T. and Sparr,E. (2015) Assembly of RNA nanostructures on supported lipid bilayers. *Nanoscale*, **7**, 583–596.
24. Lussier,A., Bastet,L., Chauvier,A. and Lafontaine,D.A. (2015) A kissing loop is important for btuB riboswitch ligand sensing and regulatory control. *J. Biol. Chem.*, **290**, 26739–26751.
25. Butcher,S.E. and Pyle,A.M. (2011) The molecular interactions that stabilize RNA tertiary structure: RNA motifs, patterns, and networks. *Acc. Chem. Res.*, **44**, 1302–1311.
26. Tuerk,C. and Gold,L. (1990) Systematic evolution of ligands by exponential enrichment: RNA ligands to bacteriophage T4 DNA polymerase. *Science*, **249**, 505–510.

27. Ellington,A.D. and Szostak,J.W. (1992) Selection in vitro of single-stranded DNA molecules that fold into specific ligand-binding structures. *Nature*, **355**, 850–852.
28. Ducongé,F. and Toulmé,J.J. (1999) In vitro selection identifies key determinants for loop–loop interactions: RNA aptamers selective for the TAR RNA element of HIV-1. *RNA*, **5**, 1605–1614.
29. Aldaz-Carroll,L., Tallet,B., Dausse,E., Yurchenko,L. and Toulmé,J.-J. (2002) Apical loop−internal loop interactions: a new RNA−RNA recognition motif identified through in vitro selection against RNA hairpins of the hepatitis C virus mRNA. *Biochemistry*, **41**, 5883–5893.
30. Watrin,M., Von Pelchrzim,F., Dausse,E., Schroeder,R. and Toulmé,J.-J. (2009) In vitro selection of RNA aptamers derived from a genomic human library against the TAR RNA element of HIV-1. *Biochemistry*, **48**, 6278–6284.
31. Ducongé,F., Di Primo,C. and Toulmé,J.-J. (2000) Is a closing 'GA pair' a rule for stable loop–loop RNA complexes? *J. Biol. Chem.*, **275**, 21287–21294.
32. Beaurain,F., Di Primo,C., Toulmé,J.J. and Laguerre,M. (2003) Molecular dynamics reveals the stabilizing role of loop closing residues in kissing interactions: Comparison between TAR-TAR* and TAR-aptamer. *Nucleic Acids Res.*, **31**, 4275–4284.
33. Van Melckebeke,H., Devany,M., Di Primo,C., Beaurain,F., Toulmé,J.-J., Bryce,D.L. and Boisbouvier,J. (2008) Liquid-crystal NMR structure of HIV TAR RNA bound to its SELEX RNA aptamer reveals the origins of the high stability of the complex. *Proc. Natl. Acad. Sci. U.S.A.*, **105**, 9210–9215.
34. Darfeuille,F., Sekkai,D., Dausse,E., Kolb,G., Yurchenko,L., Boiziau,C. and Toulme,J.J. (2002) Driving in vitro selection of anti-HIV-1 TAR aptamers by magnesium concentration and temperature. *Comb. Chem. High Throughput Screen.*, **5**, 313–325.
35. Boiziau,C., Dausse,E., Yurchenko,L. and Toulmé,J.J. (1999) DNA aptamers selected against the HIV-1 trans-activation-responsive RNA element form RNA-DNA kissing complexes. *J. Biol. Chem.*, **274**, 12730–12737.
36. Barbault,F., Huynh-Dinh,T., Paoletti,J. and Lancelot,G. (2002) A new peculiar DNA structure: NMR solution structure of a DNA kissing complex. *J. Biomol. Struct. Dyn.*, **19**, 649–658.
37. Ke,Y., Meyer,T., Shih,W.M. and Bellot,G. (2016) Regulation at a distance of biomolecular interactions using a DNA origami nanoactuator. *Nat. Commun.*, **7**, 10935.
38. Seeman,N.C., Mao,C., Sun,W. and Shen,Z. (1999) A nanomechanical device based on the B|[ndash]|Z transition of DNA. *Nature*, **397**, 144–146.
39. Andersen,E.S., Dong,M., Nielsen,M.M., Jahn,K., Subramani,R., Mamdouh,W., Golas,M.M., Sander,B., Stark,H., Oliveira,C.L.P. *et al.* (2009) Self-assembly of a nanoscale DNA box with a controllable lid. *Nature*, **459**, 73–76.
40. Modi,S., Nizak,C., Surana,S., Halder,S. and Krishnan,Y. (2013) Two DNA nanomachines map pH changes along intersecting endocytic pathways inside the same cell. *Nat. Nanotechnol.*, **8**, 459–467.
41. Li,T. and Famulok,M. (2013) I-Motif-programmed functionalization of DNA nanocircles. *J. Am. Chem. Soc.*, **135**, 1593–1599.
42. Wieland,M., Benz,A., Haar,J., Halder,K. and Hartig,J.S. (2010) Small molecule-triggered assembly of DNA nanoarchitectures. *Chem. Commun.*, **46**, 1866–1868.
43. Gong,X., Zhou,W., Chai,Y., Yuan,R. and Xiang,Y. (2016) MicroRNA-induced cascaded and catalytic self-assembly of DNA nanostructures for enzyme-free and sensitive fluorescence detection of microRNA from tumor cells. *Chem. Commun.*, **52**, 2501–2504.
44. Bujold,K.E., Fakhoury,J., Edwardson,T.G.W., Carneiro,K.M.M., Briard,J.N., Godin,A.G., Amrein,L., Hamblin,G.D., Panasci,L.C., Wiseman,P.W. *et al.* (2014) Sequence-responsive unzipping DNA cubes with tunable cellular uptake profiles. *Chem. Sci.*, **5**, 2449–2455.
45. Wu,N. and Willner,I. (2017) Programmed dissociation of dimer and trimer origami structures by aptamer–ligand complexes. *Nanoscale*, **9**, 1416–1422.
46. Westhof,E. and Patel,D.J. (1997) Nucleic acids from self-assembly to induced-fit recognition. *Curr. Opin. Struct. Biol.*, **7**, 305–309.
47. Martini,L., Ellington,A.D. and Mansy,S.S. (2016) An in vitro selection for small molecule induced switching RNA molecules. *Methods*, **106**, 51–57.
48. Nutiu,R. and Li,Y. (2003) Structure-switching signaling aptamers. *J Am Chem Soc*, **125**, 4771–4778.
49. Stoltenburg,R., Nikolaus,N. and Strehlitz,B. (2012) Capture-SELEX: selection of DNA aptamers for aminoglycoside antibiotics. *J. Anal. Methods Chem.*, **2012**, 1–14.
50. Durand,G., Lisi,S., Ravelet,C., Dausse,E., Peyrin,E. and Toulmé,J.-J. (2014) Riboswitches based on kissing complexes for the detection of small ligands. *Angew. Chem. Int. Ed.*, **53**, 6942–6945.
51. Goux,E., Lisi,S., Ravelet,C., Durand,G., Fiore,E., Dausse,E., Toulmé,J.-J. and Peyrin,E. (2015) An improved design of the kissing complex-based aptasensor for the detection of adenosine. *Anal. Bioanal. Chem.*, **407**, 6515–6524.
52. Chovelon,B., Durand,G., Dausse,E., Toulmé,J.-J., Faure,P., Peyrin,E. and Ravelet,C. (2016) ELAKCA: enzyme-linked aptamer kissing complex assay as a small molecule sensing platform. *Anal. Chem.*, **88**, 2570–2575.
53. Durand,G., Dausse,E., Goux,E., Fiore,E., Peyrin,E., Ravelet,C. and Toulmé,J.-J. (2016) A combinatorial approach to the repertoire of RNA kissing motifs; towards multiplex detection by switching hairpin aptamers. *Nucleic Acids Res.*, **44**, 4450–4459.
54. Zuker,M. (2003) Mfold web server for nucleic acid folding and hybridization prediction. *Nucleic Acids Res.*, **31**, 3406–3415.
55. Darty,K., Denise,A. and Ponty,Y. (2009) VARNA: Interactive drawing and editing of the RNA secondary structure. *Bioinformatics*, **25**, 1974–1975.
56. Bassam,B.J. and Gresshoff,P.M. (2007) Silver staining DNA in polyacrylamide gels. *Nat. Protoc.*, **2**, 2649–2654.
57. Takeuchi,Y., Endo,M., Suzuki,Y., Hidaka,K., Durand,G., Dausse,E., Toulmé,J.-J. and Sugiyama,H. (2016) Single-molecule observations of RNA-RNA kissing interactions in a DNA nanostructure. *Biomater. Sci.*, **4**, 130–135.
58. Huizenga,D.E. and Szostak,J.W. (1995) A DNA aptamer that binds adenosine and ATP. *Biochemistry*, **34**, 656–665.
59. Lin,C.H. and Patel,D.J. (1997) Structural basis of DNA folding and recognition in an AMP-DNA aptamer complex: distinct architectures but common recognition motifs for DNA and RNA aptamers complexed to AMP. *Chem. Biol.*, **4**, 817–832.
60. Chu,W., Weerasekera,A. and Kim,C.-H. (2017) On the conformational stability of the smallest RNA kissing complexes maintained through two G·C base pairs. *Biochem. Biophys. Res. Commun.*, **483**, 39–44.
61. Goux,E., Dausse,E., Guieu,V., Azéma,L., Durand,G., Henry,M., Choisnard,L., Toulmé,J.-J., Ravelet,C. and Peyrin,E. (2017) A colorimetric nanosensor based on a selective target-responsive aptamer kissing complex. *Nanoscale*, **83**, 6464–6467.
62. Barth,A., Kobbe,D. and Focke,M. (2016) DNA–DNA kissing complexes as a new tool for the assembly of DNA nanostructures. *Nucleic Acids Res.*, **44**, 1502–1513.
63. Seeman,N.C., Mao,C., LaBean,T.H. and Reif,J.H. (2000) Logical computation using algorithmic self-assembly of DNA triple-crossover molecules. *Nature*, **407**, 493–496.
64. Wang,D., Fu,Y., Yan,J., Zhao,B., Dai,B., Chao,J., Liu,H., He,D., Zhang,Y., Fan,C. *et al.* (2014) Molecular logic gates on DNA origami nanostructures for MicroRNA diagnostics. *Anal. Chem.*, **86**, 1932–1936.
65. Yang,J., Jiang,S., Liu,X., Pan,L. and Zhang,C. (2016) Aptamer-binding directed DNA origami pattern for logic gates. *ACS Appl. Mater. Interfaces*, **8**, 34054–34060.